ERDC TN-23-1
September 2023

Accelerated Corrosion of Infrastructural Seven-Strand Cables via Additively Manufactured Corrosion Flow Cells

Matthew W. Glasscott and Jason D. Ray

PURPOSE: The purpose of this project was to generate an accelerated corrosion methodology capable of producing seven-strand cables with simulated corrosive defects for calibration of nondestructive analysis (NDA) techniques. An additively manufactured accelerated corrosion cell was motivated and designed. Previous attempts at accelerated electrochemical corrosion used a large cable area with a current density that was too low (i.e., 1 A/m^2)* to effectuate efficient corrosion. The accelerated corrosion cell presented here takes advantage of the restricted area within the corrosion flow cell to maximize the corrosion rate in a consistent and calibrated manner (i.e., 2,000 A/m^2).

BACKGROUND: Corrosion (i.e., rusting) is a spontaneous electrochemical process involving a cathode (i.e., electron source) and an anode (i.e., electron sink; Glass and Buenfeld 1997). Such processes follow from the natural potential differences that arise between two metals connected via a solution phase, whether it be of high volume (e.g., a steel cable in the ocean) or low volume (e.g., an exposed bridge beam covered by a micrometer-thin layer of condensation). The corrosion process follows several fundamental steps (Robertson 1989). First, a potential gradient forms between two metal contacts based on both the intrinsic properties of the metals in question and on extrinsic factors (e.g., oxide layers). For instance, the original Statue of Liberty contained contact points between the copper exterior and the internal iron support structure (Moyer and Everett 2014). Intrinsically, copper is easier to oxidize than iron, resulting in a potential gradient. Once a potential gradient has formed, electrons begin to migrate from the cathode (higher potential) to the anode (lower potential) via charged solution species called ions. Molecules are reduced (i.e., gain electrons) at the cathode and are oxidized (i.e., lose electrons) at the anode. In solution, molecules prone to gaining electrons are generally oxygen or water, which form peroxide or hydrogen gas, respectively, upon reduction. This process occurs at the harder-to-oxidize metal, which, in the case of the Statue of Liberty, is iron. Most relevant to corrosion, zero-valent metal is readily oxidized at the anode to form solution-phase metal ions, resulting in mass loss from the anode itself. The copper exterior of the Statue of Liberty was thus oxidized to blue-green copper ions (Cu^{2+}), giving the statue its characteristic color. Thus, corrosion on the macroscale proceeds through a nanoscopic molecular process. To quench the corrosion process in the Statue of Liberty, Teflon blocks were

*For a full list of the spelled-out forms of the units of measure used in this document, please refer to *US Government Publishing Office Style Manual*, 31st ed. (Washington, DC: US Government Publishing Office, 2016), 248–252, https://www.govinfo.gov/content/pkg/GPO-STYLEMANUAL-2016/pdf/GPO-STYLEMANUAL-2016.pdf.

used to separate the copper and iron contact points, disconnecting the circuit and, thus, slowing the corrosion process.

Environmental corrosion is an energetically spontaneous, but kinetically sluggish, process; it takes years for infrastructure to experience metallic mass loss to the point of failure (e.g., a cable under tension snapping; Suzumura and Nakamura 2004). However, mass loss is not the only negative effect introduced by corrosion. For instance, when rebar cast in concrete begins to rust, the metal ions leaving the anode surface are hydrated and, thus, rapidly grow in molecular size. Multiplied over millions of molecules, the pressure exerted by this rust causes fracturing and cracking, compromising structural integrity. Therefore, methods to evaluate corrosion processes are extremely important for maximizing the lifetime of infrastructural assets (Henriksen et al. 1998). NDA techniques are ideal for this purpose because they can be readily deployed in the field and do not, by their nature, damage the asset of interest (Neslušan et al. 2019). However, such methods require ex situ corroded samples for assessment and calibration. Calibration samples may be obtained from the environment under natural corrosion conditions or directly produced by applying an external potential to a target system to drive corrosion. The latter holds the advantage of being rapid and controlled because the potential gradient and current density may be precisely modulated; this is generally referred to as *accelerated corrosion* (Austin et al. 2004; Zeng et al. 2020; Sola et al. 2019).

We proposed a method to accelerate the corrosion of seven-strand cables used in soil-rock anchor units to evaluate the feasibility of NDA techniques. A portable, 3D-printed corrosion flow cell was engineered to permit flexible evaluation of large cables (i.e., >50 ft long), which previously required high-volume corrosion reactors. We begin our discussion by evaluating this previous corrosion method and the inspiration derived from it, which led to the development of the portable corrosion flow cell. We exploited the controlled surface area afforded by the portable corrosion flow cell to calibrate the corrosion process. The cell incorporated a high-surface-area stainless steel scrubber as the cathode and drove mass loss at the steel seven-strand cable anode via a direct current (DC) power supply. Mass loss was calibrated by evaluating the reduction in cable diameter as a function of time at a set current magnitude (6A/cell), revealing a semi-exponential trend. Thus, corrosion defects may be readily introduced into seven-strand cables using this method to promote the evaluation of NDA technology for in-field use.

RESULTS: The previous US Army Engineer Research and Development Center (ERDC) accelerated corrosion method, which was described in Ebeling et al. (2016), employed multiple reactor beds filled with saturated brine to corrode seven-strand cables (Figure 1*a*). While this method proved effective for initiating pitting corrosion, long experimental timeframes were required to significantly corrode samples. We believe this may be attributed to the low current density applied to each cable during the corrosion process. Consider the corrosion circuit in Figure 1*b*, where a constant current flows through a wire and passes over multiple resistors, which represent the corrosion process leading to mass loss as Fe^{2+} ions. According to Kirchhoff's Law, the current is divided by 50% at each junction. Thus, mass loss is related both to the constant current magnitude and the material surface area. In other words, if the current is held at a constant value, a smaller surface will corrode more severely than a larger surface. This idea may be represented by the following equation:

$$Corrosion\ Rate \propto \frac{Current\ Magnitude\ (A)}{Surface\ Area\ (m^2)}. \quad (1)$$

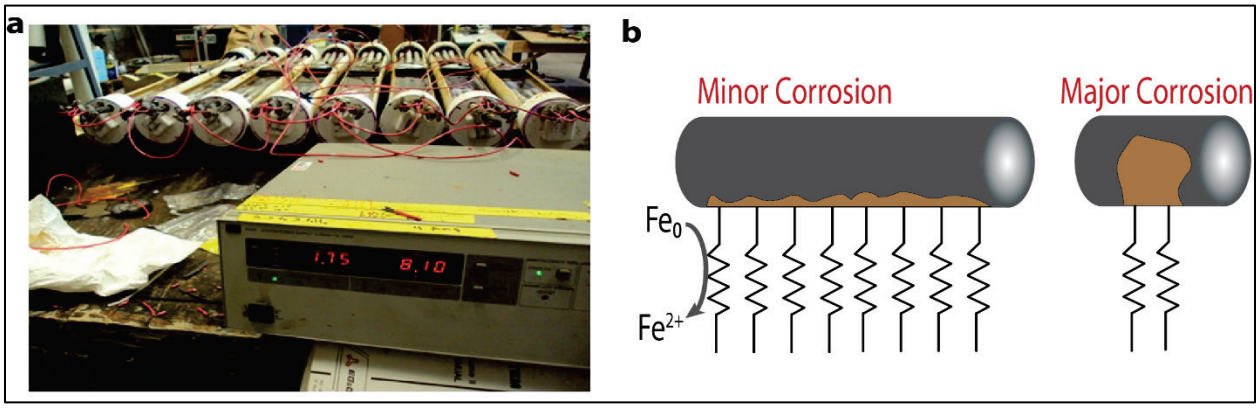

Figure 1. (*a*) Previously used accelerated corrosion apparatus using a single power supply in parallel with eight reactor beds, each containing a submerged 50 ft cable. Image reproduced from Ebeling et al. (2016, 36). (*b*) Schematic representation of Kirchoff's Law for understanding the importance of current density.

The previous accelerated corrosion method (Ebeling et al. 2016) employed a constant current magnitude of approximately 8 A, applied in parallel across several reactor beds. Assuming each reactor bed had a constant impedance, this immediately divided the current equally between each unit (i.e., if eight reactor beds were employed, as in Figure 1*a*, each would see 1 A of current), driving down the current density even further. Corroding an array of eight completely submerged 50 ft cables (assuming perfect cylinders) suggests a surface area on the order of 0.8 m^2, resulting in a current density of approximately 1 A/m^2 per cable. This value served as a benchmark for comparison to the newly developed accelerated corrosion method.

Increasing the current magnitude represents one possible solution for increasing the current density; however, several issues arise when dealing with high-current systems. First, specialized equipment is required to deal with the resistive heating incurred when passing large currents (e.g., 100 A). Wire gauges must be increased, and high-power sources or external generators become necessary because typical 120 Volts alternating current power outlets are only rated for approximately 20 A. Second, the temperature of the reactor bed must be regulated because the heat emitted under a high-current condition will change the corrosion rate, which is temperature dependent. Indeed, passing higher currents was attempted in the previous corrosion method, but the power supply overheated and failed due to a combination of the high currents and humidity. The water was also observed to increase in temperature under these conditions (as expected), which would be detrimental to reproducibly controlling the corrosion rate.

Voltage also plays an important role in the corrosion process. There are two major components to system voltage: voltage drop due directly to the corrosion process and voltage drop due to the resistance or impedance of the corrosion cell. Thermodynamically, a driving force is required to force the corrosion process to proceed at accelerated rates. For solid iron conversion to Fe^{2+}, this potential is generally less than 0.5 V. However, a high resistance in the system due to solution resistivity and junction resistance may increase the voltage necessary to pass a certain magnitude of current. As an example, corrosion processes are generally accelerated using constant current

methods, which we have employed here. DC power supplies may be compared to pumps, where the voltage is the pressure a given pump is capable of exerting, and the current is the flow rate. In constant current mode, we ask the DC power supply to exert whatever pressure or voltage is necessary to achieve a certain flow rate or current. However, if the resistance of the system is high, the power supply may be incapable of attaining the specified flow rate or current, in which case the pressure or voltage will hit a "rail" at its maximum possible value for that specific power supply. This results in a lower-than-anticipated current. Thus, it is helpful to track the voltage required to drive the corrosion process as a benchmark to ensure the anticipated current is flowing for the duration of the corrosion process.

Building on the lessons learned from the previous corrosion effort (Ebeling et al. 2016), we created a 3D-printed corrosion flow cell to isolate the corrosion process to a smaller surface area, thereby lowering the current magnitude requirements to achieve a high current density. This flow cell achieved three main objectives. First, the current density could be maximized because only a small surface area of the cable was being corroded. Second, the solution could continuously flow through the cell to remove oxidized products and maintain the pH, allowing the corrosion to proceed more efficiently. Third, because the current magnitude, surface area, and flow rate were all externally controlled, the process could be calibrated with high reproducibility.

To create the corrosion flow cell, a computer-aided design (CAD) model was generated using TinkerCAD (Figure 2*a*). The corrosion flow cell was designed as two cylinders, the outer cylinder (solid) with a length of 91.5 mm and a radius of 57 mm, and the inner cylinder (hole) with a length of 50 mm and a radius of 44 mm. Two through-holes (8.5 mm radius) were integrated to allow the cell to be fitted around a cable and caulked into place. Thus, the total accessible cable area was greatly reduced to 3.12×10^{-3} m^2 in this configuration, three orders of magnitude less than that of the previous cell. Using a current magnitude of 6 A, the theoretical current density of the corrosion flow cell was approximately 2,000 A/m^2, representing a significant increase over the previous method.

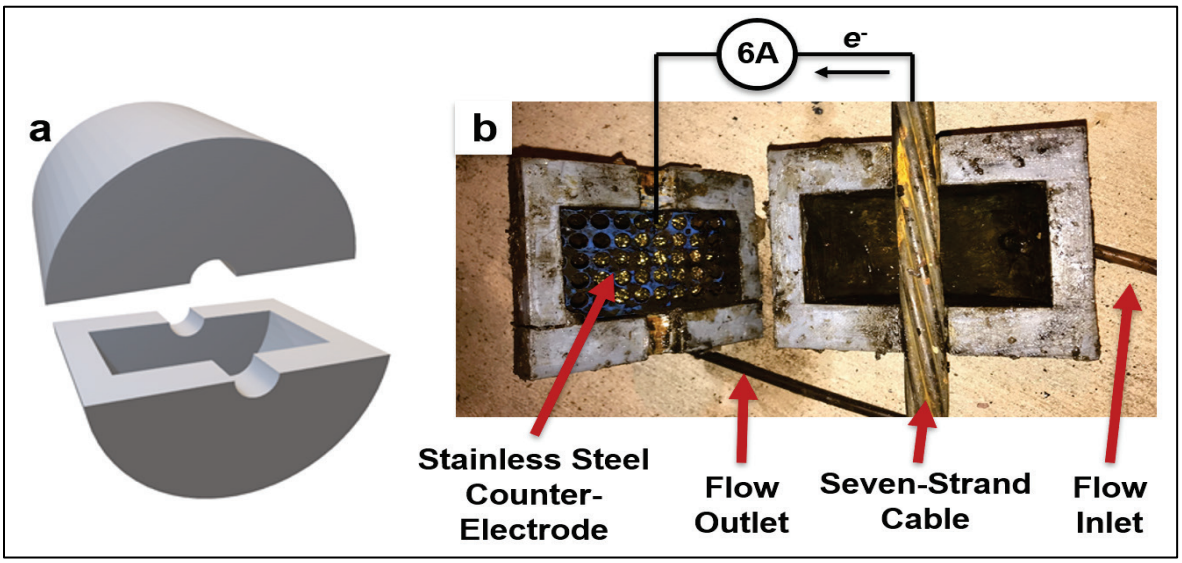

Figure 2. (*a*) A 3D-printed corrosion flow cell designed in TinkerCAD. (*b*) Image showing various components of the flow cell system with schematic representation of current flow across the unit.

Following 3D printing of the cell, additional features were added to facilitate the corrosion process (Figure 2*b*). Because both halves of the cell were equivalent when retrieved from the 3D printer, one half was labeled *top* and the other *bottom*. Two holes were drilled in the top and bottom of the unit to act as the inlet and outlet for solution flow. The hole drilled in the top was perpendicular to the plane to ensure the cell filled completely with liquid. The hole in the bottom half was drilled at 35° to the plane to allow the cell to rest on a flat surface. Flexible Tygon tubes (1/4 in. outer diameter × 1/8 in. inner diameter) that were 10 ft long were fitted to the holes and sealed in place with epoxy resin.

Because the corrosion flow cell required a counter electrode (cathode) to complete the circuit for the corrosion process occurring at the seven-strand cable (anode), a 3 in. steel nail was inserted into the top half through a drilled hole and was connected to a Scotch-Bright stainless steel metal scrubber within the corrosion flow cell. The high surface area of the stainless-steel scrubber helped lower the junction resistance of the corrosion cell and facilitated higher current magnitudes. Copper scrubber counter electrodes (higher conductivity) were also employed, but they corroded themselves and disintegrated via cathodic corrosion too quickly. While noble metals would be ideal as robust counter electrodes, the cost-effectiveness of stainless steel provided an excellent alternative and did not require replacement or completely disintegrate within the timeframe of these experiments.

The cathode and anode must not come into contact when a voltage is applied because electrons will simply take the directly conductive path and bypass the solution-based corrosion process. Thus, a plastic separator was inserted to ensure the stainless-steel scrubber cathode remained separate from the seven-strand cable anode.

The aforementioned accessories represent a completed corrosion flow cell unit, but additional infrastructure was required to control the flow rate, voltage, and current magnitude. A 55 gal. drum was employed as a reservoir to contain the corrosion matrix (5% sodium chloride, NaCl, in tap water; Figure 3). This matrix was chosen based on literature precedent (Chang et al. 2008), and it promotes corrosion via chloride attack while greatly decreasing the solution resistivity. Notably, the pH of the solution was approximately 7, which promoted the formation of iron hydroxide colloids during the corrosion process. To remove these colloids from the corrosion matrix and keep the solution clean of larger corrosion fragments that might clog the pumps, we installed a 10 µm filter bag (Pentier Industrial) in the 55 gal. drum to filter the effluent from the outlet. Because the flow rates are relatively high in this method, a large filter bag is recommended to ensure overflow does not occur. In addition, the corrosion flow cell was not entirely watertight, which prompted us to place the cell on a platform over the 55 gal. drum (or bucket) to catch the spillage. The spillage rate was generally minimal, but these recycling efforts were necessary for the longer experimental timeframes.

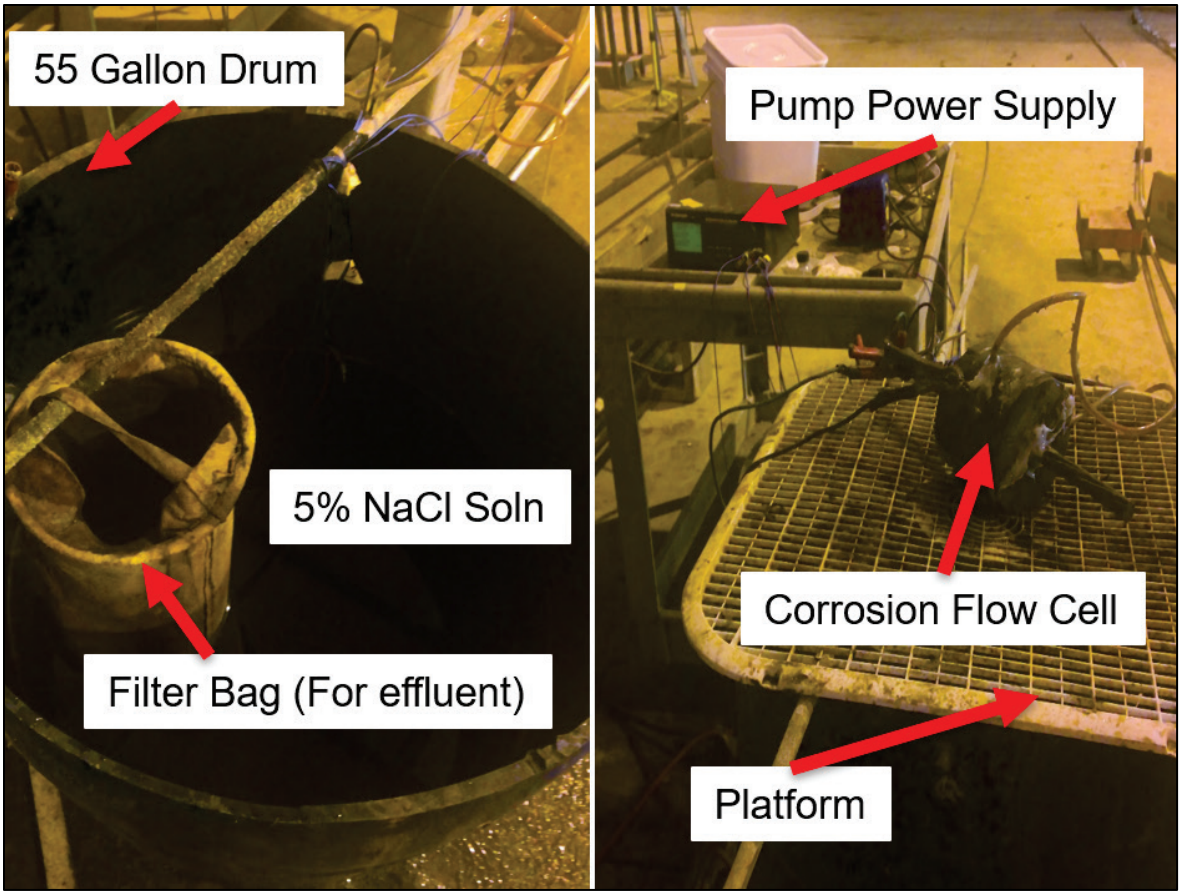

Figure 3. The corrosion matrix reservoir, filter bag to purify the effluent, and set-up of the corrosion flow cell above the reservoir.

A pump was necessary to control the flow rate of the corrosion matrix into the corrosion flow cell. For this purpose, we selected submersible 12 VDC pumps from March Pumps (part number MARCH-0893-0030-0200). These pumps are chemical resistant and brushless (which is necessary considering the corrosive nature of the solution) and have tunable flow rates depending on the DC power applied. We chose to operate these pumps at a flow rate correlated to a 0.5 A current using a BK Precision power supply. Furthermore, multiple pumps may be connected to the same power supply to multiplex the corrosion process. In this study, we used three pumps connected to three separate flow cells to simultaneously drive the process in triplicate (Figure 4). This required a current of 1.5 A from the power supply (0.5 A for each pump, split equivalently due to the equivalent impedance).

Figure 4. Multiplexed corrosion flow cells being used to corrode three separate seven-strand cables. Due to the portability of the cell, corrosion defects may be introduced at any point in the cable length without the need for large reactor beds.

Finally, a DC power supply was necessary to drive the corrosion process itself. To precisely control the corrosion process, we used a 6 A, 20 V precision DC power supply. The negative lead was connected to the cathode (i.e., nail on the outside of the corrosion cell), and the positive lead was connected directly to the seven-strand cable. The power supply was then set to continuously deliver 6.000 A, which generally required 9 to 20 V. The voltage can fluctuate as the surface area of the corroding surface decreases, but as long as the current remains constant, the process may be calibrated by evaluating the mass loss (i.e., reduction in cable diameter) as a function of corrosion timeframe.

The corrosion flow cell was calibrated under the following conditions: current magnitude 6A, voltage max 20 V, flow rate 0.5 A, matrix 5% NaCl. Figure 5*a* shows multiple seven-strand cables subjected to corrosion for various timeframes. Clearly, the longer the corrosion timeframe, the more severe the cable diameter reduction due to corrosion. Figure 5*b* shows a calibration curve

rendered from multiple corrosion runs (N = 3) fit to a second order polynomial, providing a straightforward metric to apply the accelerated cable corrosion technique in the future.

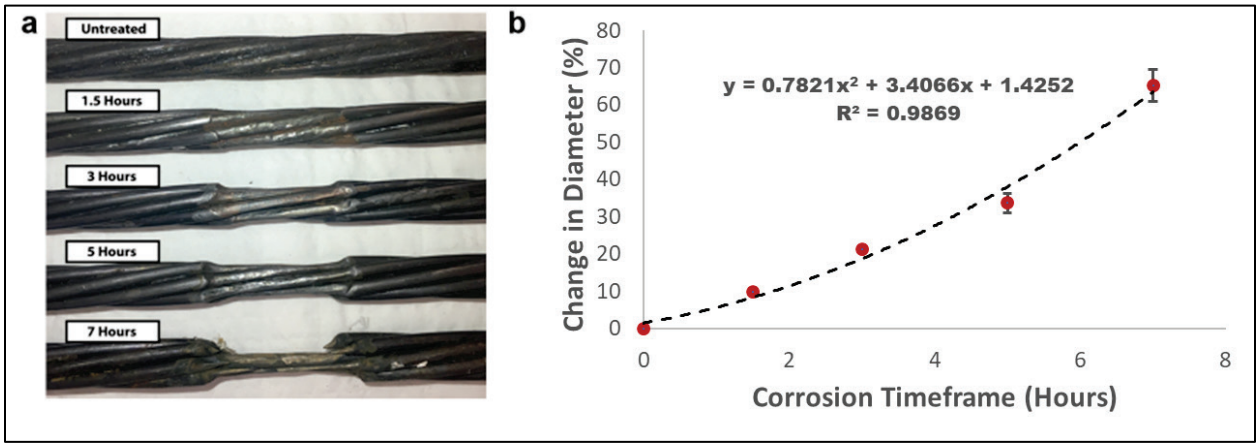

Figure 5. (*a*) Stack of corroded seven-strand cables with labeled timeframes, revealing significant mass loss over less than 10 hours. (*b*) Calibration curve showing the cable diameter reduction as a function of corrosion timeframe.

SUMMARY: An additively manufactured accelerated corrosion cell was motivated and designed. Previous attempts at accelerated electrochemical corrosion used large cable areas with a current density that was too low to effectuate efficient corrosion. The presented accelerated corrosion cell takes advantage of the restricted area within the watertight cylinder to maximize the corrosion rate in a consistent and calibrated manner. The cell was designed using an open-source TinkerCAD software and is available upon request from the corresponding author. Integration of the accelerated corrosion cell with other testing equipment (e.g., pump, effluent purification system, reservoir) permitted accelerated corrosion of seven-strand cables for future use in NDA evaluation for eventual applications in concrete diagnostics.

ADDITIONAL INFORMATION: This technical note was prepared by Dr. Matthew Glasscott of the Environmental Laboratory (EL), ERDC, and by Mr. Jason Ray of the Information Technology Laboratory (ITL), ERDC. For additional information, resources, and CAD files, please contact Dr. Matthew Glasscott, Matthew.W.Glasscott@usace.army.mil. This technical note should be cited as follows:

> Glasscott, M. W., and J. Ray. 2023. *Accelerated Corrosion of Infrastructural Seven-Strand Cables via Additively Manufactured Corrosion Flow Cells*. ERDC TN-23-1. Vicksburg, MS: US Army Engineer Research and Development Center.

REFERENCES

Austin, S. A., R. Lyons, and M. J. Ing. 2004. "Electrochemical Behavior of Steel-Reinforced Concrete During Accelerated Corrosion Testing." *Corrosion* 60 (2): 203–212. http://dx.doi.org/10.5006/1.3287722.

Chang, J. W., L. M. Peng, X. W. Guo, A. Atrens, P. H. Fu, W. J. Ding, and X. S. Wang. 2008. "Comparison of the Corrosion Behaviour in 5% NaCl Solution of Mg Alloys NZ30k and AZ91d." *Journal of Applied Electrochemistry* 38 (2): 207–214. http://dx.doi.org/10.1007/s10800-007-9426-x.

Ebeling, R. M., B. C. White, J. A. Evans, R. W. Haskins, and E. L. Miller. 2016. *Corrosion Induced Loss of Capacity of Post-Tensioned Seven Wire Strand Cable Used in Multistrand Anchor Systems Installed at Corps Projects*. ERDC/ITL TR-16-4. Vicksburg, MS: US Army Engineer Research and Development Center, Information Technology Library. http://dx.doi.org/10.21079/11681/21664.

Glass, G. K., and N. R. Buenfeld. 1997. "The Presentation of the Chloride Threshold Level for Corrosion of Steel in Concrete." *Corrosion Science* 39 (5): 1,001–1,013. https://doi.org/10.1016/S0010-938X(97)00009-7.

Henriksen, C. F., A. Knudsen, and M. W. Braestrup. 1998. "Cable Corrosion: Undetected?" *Concrete International* 20 (10): 69–72.

Moyer, R. H., and S. A. Everett 2014. "Why the Statue of Liberty Is Green: Coatings, Corrosion, and Patina." *Science Scope* 38 (1): 12–19. https://www.proquest.com/docview/1556956125?pq-origsite=gscholar&fromopenview=true.

Neslušan, M., F. Bahleda, P. Minárik, K. Zgútová, and M. Jambor. 2019. "Non-Destructive Monitoring of Corrosion Extent in Steel Rope Wires Via Barkhausen Noise Emission." *Journal of Magnetism and Magnetic Materials* 484: 179–187. https://doi.org/10.1016/j.jmmm.2019.04.017.

Robertson, J. 1989. "The Mechanism of High Temperature Aqueous Corrosion of Steel." *Corrosion Science* 29 (11): 1,275–1,291. https://doi.org/10.1016/0010-938X(89)90120-0.

Sola, E., J. Ožbolt, G. Balabanić, and Z. M. Mir. 2019. "Experimental and Numerical Study of Accelerated Corrosion of Steel Reinforcement in Concrete: Transport of Corrosion Products." *Cement and Concrete Research* 120: 119–131. https://doi.org/10.1016/j.cemconres.2019.03.018.

Suzumura, K., and S.-I. Nakamura, 2004. "Environmental Factors Affecting Corrosion of Galvanized Steel Wires." *Journal of Materials in Civil Engineering* 16 (1): 1–7. https://doi.org/10.1061/(ASCE)0899-1561(2004)16:1(1).

Zeng, L., G. Chen, and H. Chen. 2020. "Comparative Study on Flow-Accelerated Corrosion and Erosion–Corrosion at a 90° Carbon Steel Bend." *Materials* 13 (7): 1,780. http://dx.doi.org/10.3390/ma13071780.